

1                   Evaluation of Highly Enriched Uranium (HEU)  
2                   Surrogate Sources for use in Training and Modeling

3                   Z. Scholz, M. Millett, M. Schell

4                   *Department of Mechanical Engineering, United States Naval Academy, 1 Wilson Road,*  
5                   *Annapolis, MD 21412*

---

6                   **Abstract**

Surrogate radiation sources are used to test detection equipment and train security personnel in the detection and interdiction of special nuclear material (SNM). Some current surrogate sources do not accurately match SNM energy spectra, including for HEU. In this research, we propose and investigate novel source configurations for higher fidelity surrogate SNM sources using thermal neutron capture reactions that result in prompt gammas. The objective is to create a surrogate source that has a more representative spectrum, low cost, and requires minimal security, special handling, and safety precautions.

7                   *Keywords:* Surrogate source; Highly Enriched Uranium; Homeland Security;  
8                   Gadolinium.

---

9                   **1. Introduction**

10                  The threat of nuclear terrorism and warfare is on the rise with advanced  
11                  technology and adaptive terrorist groups [1]. To counter the rising threat, the  
12                  U.S. needs to continually improve the ability to interdict the entry of illicit nu-  
13                  clear material. In order to improve the training of personnel and the testing  
14                  of both equipment and protocols used in the detection of HEU and Weapons  
15                  Grade Plutonium (WGPu), this project builds upon previous research of surro-  
16                  gate SNM sources [2] to develop potentially higher fidelity, low cost, and easily  
17                  configurable SNM surrogates.

18       The current methods of identifying and detecting nuclear or radiological  
19      weapons of mass destruction (NRWMD) are primarily limited to exploiting the  
20      radioactive emissions from the nuclear materials that make up the weapon. The  
21      emissions from NRWMD comprise X-rays, gamma rays, and neutrons based on  
22      the composition of the nuclear material. The ability to detect nuclear weapon  
23      material above the natural radiation background is also dependent on the con-  
24      figuration of the material, the amount of shielding, the type of detector, the  
25      distance from the source and the counting time [2].

26       In order to enable easier and less expensive testing and training in the detec-  
27      tion of HEU and WGPu, programs use non-SNM source materials that some-  
28      what replicate the gamma energy spectrum of SNM known as surrogate SNM.  
29      While surrogate source objects have been made with small quantities of SNM to  
30      replicate the gamma signature of HEU and WGPu exactly, they are very expen-  
31      sive and difficult to handle in a test environment. This research project focuses  
32      on developing higher fidelity non-SNM source materials. With similar radioac-  
33      tive signatures, these sources may be used to test the effectiveness of equipment  
34      and protocols (though perhaps not sensor alarm algorithms), and to provide  
35      personnel training in the use of the equipment without the need for complex  
36      security credentials and radiation safety precautions related to the handling of  
37      SNM. Specifically for this research, surrogate sources will be proposed for HEU  
38      and will focus on the prominent 186 keV peak along with accompanying features.

39

#### 40     *1.1. HEU Composition*

41       The composition of nuclear weapons made of HEU is uranium enriched to  
42      roughly 93%  $^{235}U$  with the remainder  $^{238}U$  [3]. However, should the weapon  
43      be made from reprocessed uranium from a reactor, the weapon can also contain  
44      small amounts of other uranium isotopes. Each of these radioactive isotopes  
45      comprising the nuclear material for a fission weapon can be identified by their  
46      emission of gamma-rays. HEU is usually identified by its strong 186 keV gamma  
47      peak from the decay of  $^{235}U$ . With a specific gamma ray intensity of  $3.96 \times 10^7$

48  $(\text{kg}\cdot\text{s})^{-1}$ , this energy emission is highly detectable for unshielded material and  
 49 may be used to identify a possible NRWMD. If the weapon contains other ura-  
 50 nium isotopes such as  $^{232}\text{U}$ , energy peaks can then be found at 239, 510, 583,  
 51 and 2614 keV with even larger intensities [3]. The gamma spectra for natural  
 52 and uranium up to 90% enriched in  $^{235}\text{U}$  are shown in Figure 1 and show large  
 53 peaks to include 186 and 1000 keV [4].

54

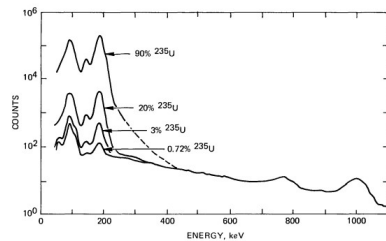


Figure 1: HEU Spectrum, obtained with a shielded 3in.  $\times$  3in. NaI detector [4].

55 *1.2. Simulating SNM*

56 There are different types of surrogate SNM sources used for replicating HEU  
 57 for testing and training. First, isotopic sources such as  $^{57}\text{Co}$  may be used, but  
 58 these do not contain an ideal match of gamma energy peaks to that of HEU. For  
 59 example,  $^{57}\text{Co}$  emits gammas at 122 and 136 keV. Second, HEU based training  
 60 sources are produced (output shown in Figure 2) at significant expense and con-  
 61 tain  $^{235}\text{U}$  and  $^{238}\text{U}$ . Such an HEU training source gives off a gamma spectrum  
 62 that matches that of HEU, but requires handling security and is prohibitively  
 63 expensive for many applications.

64

65 Both these methods of simulating weapons material rely on the emission  
 66 of gamma rays in the process of radioactive decay. This gamma radiation is  
 67 emitted in a nuclear deexcitation after a radioactive decay process results in an  
 68 excited daughter radionuclide. This research project rather focuses on a process  
 69 in which prompt gamma rays result from deexcitation following neutron capture

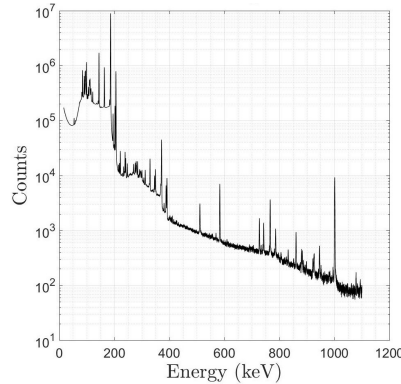


Figure 2: HPGe Spectrum from an HEU Training Source

70 in a suitable isotope.

71

72 Figure 3 displays a notional application that uses neutron capture in non-  
 73 uranium isotopes along with depleted uranium ( $^{238}U$ ) to simulate an HEU  
 74 source. When a neutron is captured, the target nucleus is placed into an excited  
 75 state and then emits gammas when returning to the ground state. The applica-  
 76 tion is inlaid over a suitcase to represent that this configuration could be used  
 77 to replicate the gamma energy spectrum of HEU that is being transported out  
 78 of regulatory control.

79

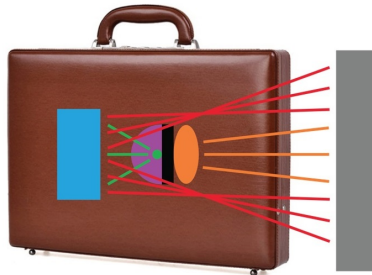


Figure 3: Notional Surrogate Configuration

80 *Displayed are the target isotope (blue), capture gammas (red), neutron source  
 81 and incident neutrons (green), borated polyethylene neutron shield (black), neu-*

<sup>82</sup> tron moderator (purple),  $^{238}\text{U}$  background gamma source (orange), and the de-  
<sup>83</sup> tector or test region (grey).

<sup>84</sup> **2. Experimental Procedure**

<sup>85</sup> Target materials for this research project were picked based on the energy  
<sup>86</sup> level of the gammas emitted through neutron capture and how close they are in  
<sup>87</sup> comparison to HEU's 186 keV peak. This, along with a consideration of addi-  
<sup>88</sup> tional undesired signatures, determined their capability of providing a gamma  
<sup>89</sup> spectrum that closely matched HEU.

<sup>90</sup>

<sup>91</sup> Research began with an analysis of data for potential target isotopes col-  
<sup>92</sup> lected from the Evaluated Nuclear Structure Data File (ENSDF) [5], Exper-  
<sup>93</sup> imental Unevaluated Nuclear Data List (XUNDL) [6], International Atomic  
<sup>94</sup> Energy Agency (IAEA) Capture Gamma Database [7], and Thermal Neutron  
<sup>95</sup> Capture Gamma Ray database [8]. Materials were selected, test configurations  
<sup>96</sup> were prepared, and testing was conducted to measure and compare generated  
<sup>97</sup> signals using both HPGe and NaI sensors.

<sup>98</sup>

<sup>99</sup> *2.1. Target Isotope Evaluation for HEU Simulation*

<sup>100</sup> Using the IAEA Capture Gamma Database, analysis was first performed by  
<sup>101</sup> narrowing possible target isotopes to within a 10 keV range of 186 keV. Isotopes  
<sup>102</sup> were further narrowed down by the relative intensity of additional interfering  
<sup>103</sup> capture gammas. It is critical to ensure that the selected target isotopes, along  
<sup>104</sup> with other naturally occurring isotopes, do not emit other gamma energies with  
<sup>105</sup> a high intensity unassociated with SNM emissions in order to achieve a high-  
<sup>106</sup> fidelity surrogate source. Of the isotopes narrowed down in this screening,  $^{157}\text{Gd}$   
<sup>107</sup> appeared favorable with a neutron capture gamma at 182 keV and an intensity  
<sup>108</sup> of 100%. Other isotopes that showed high potential for use included  $^{65}\text{Cu}$ ,  
<sup>109</sup>  $^{164}\text{Dy}$ ,  $^{161}\text{Dy}$ , and  $^{167}\text{Er}$ , giving off neutron capture gammas at 186, 184, 185,

and 184 keV respectively, all with an intensity of 100%. Target isotopes that passed this initial screening were then examined for high neutron capture cross sections in order to facilitate higher gamma production with the given neutron sources.  $^{157}\text{Gd}$  stood out in this selection with a significantly higher neutron cross-section of 254,770 barns at a neutron energy of 0.025 eV. Copper was eliminated based on capture cross section but testing with copper was conducted to verify the removal of this material from consideration.

Further evaluation came in the form of examining the chosen elements abundance on Earth [9] as well as the isotope abundance [10]. The use of these factors as part of the selection process was to minimize the cost of the surrogate source. Should an element and isotope be highly available, the cost to the end user would be much smaller. Finally, atomic density was calculated in order to determine a macroscopic cross section for capture. These variables were then normalized, creating a similar scaling system and measurable way to rank the chosen isotopes for their feasibility as an HEU surrogate source. At the end of this stage, the top three target materials were selected for testing: gadolinium, dysprosium, and erbium.

127

## 128 *2.2. $k_0$ Formulation*

Further analysis came in the form of the  $k_0$  formulation. The  $k_0$  formulation provides an accurate analytical comparison tool to evaluate yield values for gamma rays emitted from isotopes. Introduced by De Corte and Simonits in their publication Biological Trace Element Research [11], the formulation is used in activation analysis as the product of the yield and cross-section can usually be measured with greater accuracy than either parameter alone. The value of  $k_0$  for any particular gamma ray emitted from isotope i is thus defined relative to hydrogen on a mass scale, as outlined in Equations 1 and 2. For these equations,  $\sigma_{\gamma}^{z,i}(E)$  is the partial elemental cross-section in barns for the production of gamma rays of energy  $E_{\gamma}$  from element Z and isotope i.  $A_r(Z)$  represents the relative atomic weight of element Z. The equation is condensed

<sup>140</sup> by substituting in the values for hydrogen and its 2223 keV peak in Equation 2.

<sup>141</sup>

$$k_0(E_\gamma) = \frac{\frac{\sigma_\gamma^{z,i}(E_\gamma)}{A_r(Z)}}{\frac{\sigma_\gamma^H(2223\text{ keV})}{A_r(H)}} \quad (1)$$

<sup>142</sup>

$$k_0(E_\gamma) = 3.03 \times \left[ \frac{\sigma_\gamma^{z,i}(E_\gamma)}{A_r(Z)} \right] \quad (2)$$

<sup>143</sup> In comparing the  $k_0$  values for the individual target material's neutron cap-  
<sup>144</sup> ture gammas, the gammas with a  $k_0$  value greater than 10% of the largest value  
<sup>145</sup> for that element are recognized as prominent. The use of the  $k_0$  formulation  
<sup>146</sup> thus allows for an analysis of the both prompt and prominent gamma rays that  
<sup>147</sup> are being emitted by the gadolinium, dysprosium, and erbium target materials.

<sup>148</sup>

### <sup>149</sup> 2.3. Database Analysis

<sup>150</sup> The majority of the results and discussion of this paper also rely on the  
<sup>151</sup> Evaluated Gamma Ray Activation File (EGAF), a database of roughly 32,000  
<sup>152</sup> adopted prompt gamma rays for stable isotopes ranging from hydrogen to ura-  
<sup>153</sup> nium. Cataloged and consolidated by IAEAs publication of Database of Prompt  
<sup>154</sup> Gamma Rays from Slow Neutron Capture for Elemental Analysis, analysis can  
<sup>155</sup> be directly made between the spectra taken of the manufactured surrogate  
<sup>156</sup> sources and their tabulated prompt and decay gamma rays from thermal neu-  
<sup>157</sup> tron capture. Specifically for this research, tables were reproduced from this  
<sup>158</sup> publication highlighting the gamma rays from thermal neutron capture within  
<sup>159</sup> 10% of the most intense transitions. The tables were generated separately for  
<sup>160</sup> each element and were ordered by gamma ray energy. Each gamma ray was  
<sup>161</sup> specified with isotopic identification, energy and uncertainty in keV, as well as  
<sup>162</sup> partial elemental cross-sections and  $k_0$ , and their uncertainties.

### <sup>163</sup> 2.4. Surrogate Configuration Optimization

<sup>164</sup> Once the list of anticipated signatures from available isotopes was created,  
<sup>165</sup> the Monte Carlo N-Particle Transport Code (MCNP)[12] was then used to eval-

166 uate several possible configurations in which a neutron source and target ma-  
167 terial could be positioned. It was determined that in order to increase neutron  
168 economy and overall neutron capture reaction rate, the neutron source must  
169 be moderated and surrounded by the target material. Possible configurations  
170 considered included cylinders and spheres.

171

172 Evaluating these configurations led to the selection of a spherical geome-  
173 try, containing both the neutron source and a spherical polyethylene moderator  
174 within the target shell. The spherical geometry was selected due to several  
175 factors, including that a symmetrical geometry allows for the surrogate to pro-  
176 duce an isotropic response. The high neutron economy gained from a spherical  
177 geometry was also a big advantage. The polyethylene sphere was then opti-  
178 mized within MCNP, as shown in Figure 4, to determine the appropriate radius  
179 required to moderate the source neutrons to a thermal energy range for each  
180 target material shell. This modeling was performed for gadolinium, dysprosium,  
181 and erbium, to maximize emission in the range of a 186 keV gamma.

182

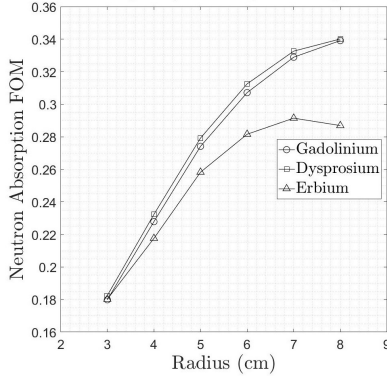


Figure 4: MCNP - Polyethylene Sphere Optimization

183 The moderation decreases the neutron energy and increases the reaction rate  
184 as the cross sections for neutron capture increase as the inverse of neutron veloc-  
185 ity at lower neutron energies. The analysis led to the selection of a 7 cm radius

186 polyethylene sphere, containing the neutron source and surrounded by the tar-  
187 get material. The polyethylene sphere was further enhanced in its fabrication  
188 with a lead capsule that surrounds the neutron source. This additional lead  
189 shielding lowers the gamma contamination that comes from the neutron source  
190 itself but also lowers the moderator thickness by approximately 2 cm so the test  
191 configuration was not optimal. Based on the proposed geometry, a polyethylene  
192 sphere with a lead capsule was fabricated by the Naval Academys engineering  
193 shop as shown in Figure 5. This sphere contains the neutron source at its cen-  
194 ter, with lead surrounding the neutron source and polyethylene surrounding the  
195 lead capsule. The sphere thermalizes neutrons from the source, minimizes the  
196 gamma contamination from the neutron source, maximizes neutron economy,  
197 and allows for an isotropic response. For future testing, a larger moderating  
198 sphere may be desirable to reduce the neutron leakage above thermal energy,  
199 allowing the neutron signature at the sensor to be reduced or eliminated.

200



Figure 5: Polyethylene Sphere with Lead Sleeve

201 Further optimization was then conducted in order to determine the best  
202 thickness of target material to surround both the polyethylene and neutron  
203 source. This optimization focused on increasing the thickness to have a larger  
204 probability of capture as well as decreasing the thickness to minimize self-  
205 shielding of the capture gamma produced. A Figure of Merit (FOM) was used  
206 that is simply the product of the neutron absorption probability and the gamma

207 transmission probability. This modeling was performed for gadolinium, dyspro-  
 208 sium, and erbium, for a 186 keV gamma. This optimization is shown in Figure 6  
 209 and resulted in an optimal thickness of less than 1 mm for most target materials.  
 210 Note that the optimum thickness is not shown for gadolinium and dysprosium,  
 211 but fabrication limitations restricted the projects interest below 1 mm thick-  
 212 ness. If a future design were to use foil materials, a thinner target may exhibit  
 213 higher effectiveness.

214

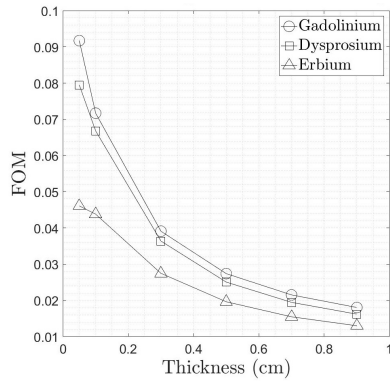


Figure 6: MCNP - Metal Hemisphere Thickness Optimization

215 As an accompanying comparison calculation, it was determined that the  
 216 mean free path for absorption of a thermal neutron in  $^{157}\text{Gd}$  was 0.0013 mm,  
 217 0.12 mm for  $^{164}\text{Dy}$ , and 0.47 mm for  $^{167}\text{Er}$ . Furthermore, examination of the iso-  
 218 topes individual mass absorption coefficients for gamma rays showed acceptable  
 219 loss for a 186 keV gamma intensity through 1 mm of the respective element. As  
 220 an example, the  $^{157}\text{Gd}$  181.94 keV gamma should retain 98.43% of its original  
 221 intensity after passing through the target material. The trend shown in Figure  
 222 6 agrees with these calculations, as the FOM increases to the smallest thickness  
 223 simulated (0.5 mm) for all three materials.

224

<sup>225</sup>      *2.5. Target Material Build*

<sup>226</sup>      The three target isotopes of highest interest, gadolinium, dysprosium, and  
<sup>227</sup>      erbium, were purchased as ingots and fabricated to form an approximately 1  
<sup>228</sup>      mm thick hemisphere. As all three materials are pyrophoric, the fabrication  
<sup>229</sup>      proved to be challenging. Starting with gadolinium, powder was produced from  
<sup>230</sup>      the ingots through a process of hammering and chiseling. For all metal fabrica-  
<sup>231</sup>      tion, regular methods such as milling and casting were not possible due to the  
<sup>232</sup>      pyrophoric nature of the materials. Once the gadolinium was powdered, pack-  
<sup>233</sup>      ets were fabricated, containing an approximate 1 mm thick layer of gadolinium  
<sup>234</sup>      powder on the adhesive side of tape with another layer of tape placed over that.  
<sup>235</sup>      A plastic vacuum mold was then used to form a plastic mold of the desired  
<sup>236</sup>      hemisphere size for the target material, and the tape gadolinium packets were  
<sup>237</sup>      placed onto the mold.

<sup>238</sup>

<sup>239</sup>      In its final form, the surrogate configuration consisted of the neutron source,  
<sup>240</sup>      lead capsule, polyethylene sphere, plastic vacuum mold, and the taped gadolin-  
<sup>241</sup>      ium packets. Shown in Figure 7 is both the fabricated polyethylene sphere and  
<sup>242</sup>      an approximate 1 mm thick, hemispherical gadolinium target material. At this  
<sup>243</sup>      stage of the research, the target material was only fabricated to be a hemisphere  
<sup>244</sup>      in order to validate the prototype design, whereas the final design recommen-  
<sup>245</sup>      dation is spherical.

<sup>246</sup>



Figure 7: Gadolinium Surrogate

<sup>247</sup>      Advances in prototype production allowed for the fabrication of the dyspro-

248 sium and erbium target materials to maintain a more rigid structure in com-  
249 parison to the gadolinium target material. For erbium and dysprosium, it was  
250 discovered that slow milling was a viable precursor for creating a powder of each  
251 of the materials. By creating chips of metal from the ingots, powder was easily  
252 created through hammering. Once the powder was acquired for both materials,  
253 plastic hemispherical molds were once again made using a plastic vacuum mold.  
254 Rather than use taped packets, however, the surrogates instead were made of  
255 two plastic hemispherical molds, one inner and one outer, with the 1 mm thick  
256 layer of material entrapped between the two using an adhesive synthetic poly-  
257 mer mixture. This surrogate setup allowed for easier handling as well as a more  
258 rigid structure. Shown in Figure 8, the dysprosium and erbium target materials  
259 resemble the gadolinium regarding the radius of the hemisphere and thickness  
260 of the material.

261



Figure 8: Dysprosium (Top) and Erbium (Bottom) Target Material Hemispheres

262 **3. Results and Discussion**

263 Following the fabrication of the prototype surrogate sources, testing was  
264 performed with an Ortec IDM-200V HPGe detector and with a 7.62 cm cylin-  
265 drical NaI detector. This experiment also made use of lead bricks to minimize

266 the background signature. The experiments performed using this setup yielded  
 267 good results, as shown in Figure 9. Taken with the gadolinium as the target  
 268 material, the figure shown is a background adjusted spectrum of the experiment  
 269 with 170 g of 99.5% pure gadolinium and an AmBe neutron source. Of note,  
 270 the y-axis is linear in an effort to express the large peak seen at 181 keV. With  
 271 the noticeable peak, this figure validates the previous work done on the target  
 272 isotope evaluation. The live time for the primary spectrum was 21600 s with  
 273 a dead time of 2.18%. The background spectrum was of the same exact setup  
 274 without the gadolinium and had a live time of 21600 s with a dead time of 1.91%.  
 275 Note that the background correction seen in Figure 9 represents a source con-  
 276 figuration where all gamma interference from the neutron source is removed; a  
 277 configuration not tested in this work but achievable through additional neutron  
 278 source shielding. The lead sleeve shown in Figure 5 had a thickness of approx-  
 279 imately 2 cm and a thicker or higher density sleeve is recommended in future  
 280 designs.

281

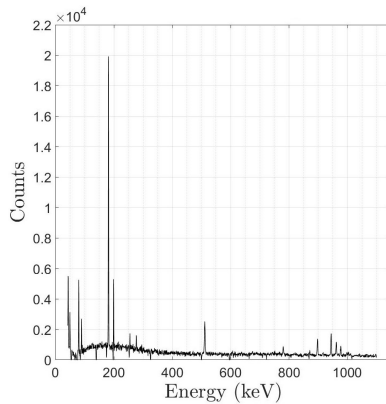


Figure 9: Gadolinium Prototype Surrogate Source Spectrum, Source Background Corrected

282 *3.1. Gadolinium*

283 Though initial testing used an AmBe neutron source, final testing used a  
 284 californium source with a strength of approximately  $4 \times 10^6$  neutrons/s. The

285 testing began with the gadolinium target material. Using a  $^{252}\text{Cf}$  source, the  
 286 complete surrogate source was placed a distance of 50 cm from the face of the  
 287 target material to the face of the HPGe detector. The complete surrogate source  
 288 includes the polyethylene sphere,  $^{252}\text{Cf}$  source, and target material. Lead bricks  
 289 were used in an effort to minimize background noise. Testing was run for 16000  
 290 seconds on the Gadolinium surrogate, which had a dead time of 24.56%. The  
 291 resulting spectrum is shown in Figure 10.

292

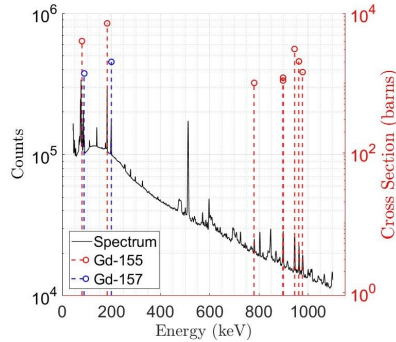


Figure 10: Gadolinium Surrogate Source Spectrum

293 Plotted alongside the spectrum are cross sectional data taken from the  
 294 Prompt Gamma-ray Neutron Activation Analysis (PGAA) [13] software, which  
 295 is derived from the isotopic measurements compiled in the ENSDF. Of note, the  
 296 182 keV capture gamma peak contained a net peak area of 569,617 ( $+/- 1292$ )  
 297 counts. This capture gamma is respectively recorded as having a cross section  
 298 of 7,200 barn, the most significant cross section of the 390 capture gammas  
 299 recorded for the  $^{157}\text{Gd}$  isotope.

300

301 Comparison between the gadolinium surrogate spectrum and an HEU training  
 302 source is provided in both Figure 11 with an HPGe detector and Figure 12  
 303 with a NaI detector. Figure 11 indicates the potential for the gadolinium surro-  
 304 gate in that it provides a close match of gamma energy peaks to that of HEU. In  
 305 its current state, the gadolinium surrogate provides a higher fidelity spectrum

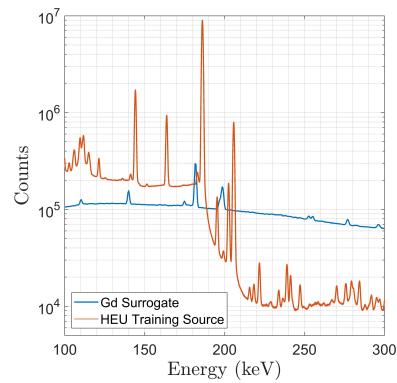


Figure 11: Gadolinium Surrogate Source Spectrum versus HEU Training Source Spectrum

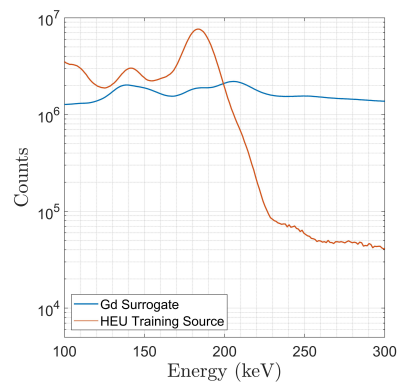


Figure 12: Gadolinium Surrogate Source Spectrum versus HEU Training Source Spectrum with an NaI Detector

306 than  $^{57}\text{Co}$  to HEU. Specifically for Figure 12, a direct comparison in spectra re-  
307 quired the count times to be normalized due to a low live time when measuring  
308 the spectrum of the HEU training source. With count times normalized, the  
309 peak height for the gadolinium surrogate test configuration is approximately an  
310 order of magnitude below that of the HEU training source, indicating that the  
311 neutron source strength would need to be increased to approximately  $4 \times 10^7$   
312 neutrons per second to provide a source strength that matches the HEU training  
313 source emission strength. The use of a stronger californium source would, how-  
314 ever, also necessitate more polyethylene and lead shielding within the surrogate.

315

316 Improvements in the gadolinium surrogate spectrum to simulate HEU may  
317 come in many forms. As shown in Table 1, the isotopic abundance ( $\sigma$ ) for  
318  $^{157}\text{Gd}$  is 15.65%, the third largest isotope percentage of the six stable isotopes  
319 for gadolinium. Of note, however, is that the thermal absorption cross section  
320 of the  $^{157}\text{Gd}$  isotope, 254,000 barns, is nearly four times larger than the next  
321 closest isotope of  $^{155}\text{Gd}$  at 60,900 barns.

322

Table 1: Gd Isotopic Abundance and Respective Cross-section for Neutron Capture

Isotope	$\Theta(\%)$	$\sigma_{\gamma}^z(b)$	$N_{\gamma}$
152	0.20(1)	735(20)	503
154	2.18(3)	85(12)	329
155	14.80(12)	60900(500)	324
157	15.65(2)	254000(800)	390
158	24.84(7)	2.2(2)	20
160	21.86(19)	1.4(3)	98

323 The first future enhancement to be considered for this project is enrichment.  
324 If a surrogate source is enriched to more than 90%  $^{157}\text{Gd}$ , the peaks shown in  
325 Figure 11 at 89 and 191 keV will be comparatively minor as they are created  
326 by the capture of neutrons in the  $^{155}\text{Gd}$  isotope. By effectively minimizing the

Table 2: Prominent Gd Neutron Capture Gammas

Isotope	$E_\gamma(\text{keV})$	$\sigma_\gamma^z(b)$	$k_o$
157	79.5100(10)	4010(100)	77.3(19)
155	88.9670(10)	1380(40)	26.6(8)
157	181.931(4)	7200(300)	139(6)
155	199.2130(10)	2020(60)	38.9(12)
157	780.174(10)	1010(22)	19.5(4)
157	897.502(10)	1200(50)	23.1(10)
157	897.611(10)	1090(50)	21.0(10)
157	944.174(10)	3090(70)	59.5(13)
157	962.104(10)	2050(130)	39.5(25)
157	977.121(10)	1440(21)	27.8(4)
157	1107.612(9)	1830(40)	35.3(8)
157	1119.163(10)	1180(30)	22.7(6)
157	1119.163(10)	1180(30)	22.7(6)
157	1183.968(10)	958(60)	18.5(12)
157	1185.988(9)	1600(90)	30.8(17)
157	1187.122(9)	1420(90)	27.4(17)
157	6750.11(5)	965(30)	18.6(6)

327 extraneous gadolinium neutron capture gammas, all of which feature relatively  
 328 strong cross sections, the spectrum will likely feature a larger peak at the desired  
 329 gamma ray energy of 182 keV. Table 2 outlines the prominent capture gammas  
 330 and their respective isotope numbers for gadolinium. Prominent capture gam-  
 331 mas, mentioned previously, are considered to be the gamma rays with a  $k_0$  value  
 332 greater than 10% of the largest value for that element. It is also important to  
 333 consider that, though not shown in this table, there are 1664 neutron capture  
 334 gammas listed in the PGAA database for gadolinium of which many still feature  
 335 a significantly strong cross section for neutron capture.

336

337     The second enhancement that could benefit this surrogate is additional lay-  
338     ering of polyethylene moderator either inside or outside of the target material  
339     shell. Additional polyethylene would increase the thermal flux at the target,  
340     and, if placed outside the target, could provide some shielding against low en-  
341     ergy interfering gamma rays from neutron capture with the  $^{157}\text{Gd}$  isotope. Opti-  
342     mization of any outside moderating material will also need to consider shielding  
343     effects on the desired 182 keV gamma.

344

345     *3.2. Dysprosium*

346     Testing with dysprosium was similar to that of the gadolinium surrogate  
347     testing. The complete surrogate was placed 50 cm away from the HPGe detec-  
348     tor with the distance marking the measurement between both faces. Testing  
349     was run for a live time of 16,000 seconds for the dysprosium surrogate with the  
350     test yielding a 24.97% dead time. The resulting spectrum is shown in Figure 13.

351

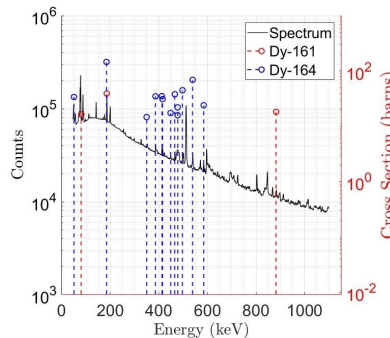


Figure 13: Dysprosium Surrogate Source Spectrum

352     The plotted spectrum shown indicates the signature captured from dyspro-  
353     sium target material in the complete surrogate setup. Interestingly, the peak  
354     of interest in this spectrum is effectively a combination of two thermal neutron  
355     capture gammas from two different isotopes of dysprosium. The two gamma  
356     rays have energies of 184 and 185 keV with elemental cross-sections of 146 and

<sup>357</sup> 39.1 barns resulting from  $^{164}\text{Dy}$  and  $^{161}\text{Dy}$ , respectively. The peak shown in the  
<sup>358</sup> spectrum has a full width at half maximum (FWHM) amplitude of 1.31 keV,  
<sup>359</sup> effectively combining the two gamma rays into a single peak. The net peak area  
<sup>360</sup> is 569,617 (+/- 1292) counts.

<sup>361</sup> In its current form, the strength of dysprosium target material comes from  
<sup>362</sup> the combined peak of the two gamma rays. Featuring isotopic abundances of  
<sup>363</sup> 18.91 and 28.18% for  $^{161}\text{Dy}$  and  $^{164}\text{Dy}$ , respectively, the two isotopes combine for  
<sup>364</sup> an elemental cross-section of 3250 barns out of the total 3666 barns for neutron  
<sup>365</sup> capture gamma production. The dysprosium isotopic data, respective cross-  
<sup>366</sup> sections for neutron capture gammas, and number of neutron capture gammas  
<sup>367</sup> listed per isotope is further shown in Table 3.

<sup>368</sup>

Table 3: Dy Isotopic Abundance and Respective Cross-section for Neutron Capture

Isotope	$\Theta(\%)$	$\sigma_{\gamma}^z(b)$	$N_{\gamma}$
156	0.06(1)	33(3)	25
160	2.34(8)	55(3)	100
161	18.91(24)	600(25)	78
162	25.51(26)	194(10)	328
163	24.90(16)	134(7)	45
164	28.18(37)	2650(70)	271

<sup>369</sup> The dysprosium surrogate could also benefit from a few enhancements. Com-  
<sup>370</sup> pared to the gadolinium surrogate, the prominence of the desired 184 and 185  
<sup>371</sup> keV neutron capture gammas are not as strong. Shown in Table 4 are the  
<sup>372</sup> prominent neutron capture gammas and their respective dysprosium isotopes  
<sup>373</sup> and elemental cross sections. Much of the difference between the gadolinium  
<sup>374</sup> and dysprosium surrogate can be directly attributed to the fraction of elemental  
<sup>375</sup> cross section for the specific neutron capture gammas being examined. With  
<sup>376</sup> the  $^{157}\text{Gd}$  peak at 182 keV featuring a 7200 barn cross-section, there is a dif-  
<sup>377</sup>ference of up to two orders of magnitude to that of the dysprosium gammas.

Table 4: Prominent Dy Neutron Capture Gammas

Isotope	$E_\gamma(keV)$	$\sigma_\gamma^z(b)$	$k_o$
164	50.4310(20)	33.9(15)	0.63(3)
161	80.64(7)	16.5(5)	0.308(9)
164	184.257(4)	146(15)	2.7(3)
161	185.19(9)	39.1(12)	0.729(22)
164	349.248(10)	14.7(6)	0.274(11)
164	385.9840(20)	34.8(10)	0.649(19)
164	411.651(5)	35.1(10)	0.655(19)
164	414.985(7)	31(5)	0.58(9)
164	447.893(7)	17.4(5)	0.324(9)
164	465.416(6)	38.0(10)	0.709(19)
164	477.061(6)	22(7)	0.41(13)
164	477.08(4)	15.8(5)	0.295(9)
164	496.931(5)	44.9(11)	0.837(21)
164	538.609(8)	69.2(19)	1.29(4)
164	583.982(5)	24(7)	0.45(13)
161	882.27(6)	18.3(6)	0.341(11)
164	5142.29(3)	15.7(10)	0.293(19)
164	5557.26(3)	28.7(14)	0.54(3)
164	5607.69(3)	35.9(16)	0.67(3)

378 In order to compensate for this difference, a dysprosium surrogate should be  
 379 enriched to 90+% in  $^{161}\text{Dy}$ .  $^{161}\text{Dy}$  is specifically desired over the other isotopes  
 380 due the number of neutron capture gammas listed for the isotope in the PGAA  
 381 database. With only 78 neutron capture gammas listed, the  $^{161}\text{Dy}$  isotope has  
 382 less than one third of the  $^{164}\text{Dy}$  isotope's gammas. While the  $^{161}\text{Dy}$  isotope  
 383 does not offer as large an elemental cross-section as  $^{164}\text{Dy}$ , what it lacks in  
 384 cross-section can be made up for an increase in neutron flux.  
 385

386     3.3. *Erbium*

387     Testing was performed on the erbium target material similar to the previous  
388     two tests. Using the complete surrogate configuration of the polyethylene  
389     sphere,  $^{252}\text{Cf}$  neutron source, and target material set at a distance of 50 cm to  
390     the face of the detector, a test was run for 16,000 seconds with a recorded dead  
391     time of 24.28%. The resulting spectrum is shown in Figure 14.

392

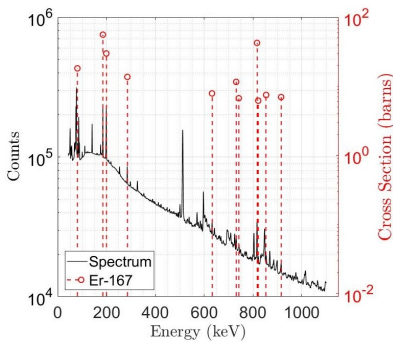


Figure 14: Erbium Surrogate Source Spectrum

393     The plotted spectrum features the desired peak of 184 keV from the  $^{167}\text{Er}$   
394     isotope with peak analysis software computing a net peak area of 384410 (+/-  
395     1206) counts. The spectrum also has another strong peak within 20 keV of the  
396     desired peak, at 198 keV. Shown in Table 5, the isotopic abundance, respective  
397     elemental cross-sections, and number of neutron capture gammas per isotope  
398     are listed for erbium. Of note, nearly all thermal neutron gammas registering  
399     in the spectrum above are created by the  $^{167}\text{Er}$  isotope, which has an isotopic  
400     abundance of 22.93% and is the third largest stable isotope of erbium. This is  
401     backed up by the PGAA database, listing the  $^{167}\text{Er}$  isotope as having 805 sep-  
402     arate neutron capture gammas, an overwhelmingly majority of the total listed  
403     neutron capture gammas for erbium at 73.72% of the total, 1092.

404

405     The erbium surrogate is flawed much in the same as the dysprosium in re-  
406     gards to the overall cross section available for neutron capture gammas. The

Table 5: Er Isotopic Abundance and Respective Cross-section for Neutron Capture

Isotope	$\Theta(\%)$	$\sigma_{\gamma}^z(b)$	$N_{\gamma}$
162	0.14(1)	19(2)	1
166	33.61(35)	16.9(16)	87
167	22.93(17)	649(8)	805
168	26.78(26)	2.74(8)	102
170	14.93(27)	8.9(3)	97

407 prominent neutron capture gammas and their respective erbium isotopes and  
 408 elemental cross sections are outlined along with  $k_0$  values in Table 6. At natural  
 409 abundance, the desired neutron capture gamma of 184 keV is at 8.04% of the  
 410 total cross section available. Should the surrogate be made of 100% enriched  
 411  $^{167}\text{Er}$ , this percentage would only increase to 8.63%. From this calculation,  
 412 the cost required for enrichment of the erbium metal would yield little value.  
 413 The erbium surrogate is further flawed by the strength of the cross-sections for  
 414 other prominent neutron capture gammas in  $^{167}\text{Er}$ . As mentioned previously,  
 415 the  $^{167}\text{Er}$  isotope has a peak at 198 keV with a cross-section that is close to half  
 416 that of the desired 184 keV peak. There may not be enhancements to improve  
 417 an erbium surrogate's spectral match of HEU.

418

#### 419 3.4. Natural Uranium

420 Spectra were also obtained for natural uranium using fuel slugs from the  
 421 Naval Academys sub-critical reactor. These experiments were focused on qual-  
 422 ifying the 766 keV and 1 MeV peaks from natural uranium to augment the  
 423 prompt capture gamma source, as suggested in the notional configuration in  
 424 Figure 3. The addition of this signature will improve the fidelity of the gamma  
 425 spectrum to more closely match that of HEU in the higher energy region. Fig-  
 426 ure 15 shows the natural uranium spectrum taken by a high purity germanium  
 427 detector.

428

Table 6: Prominent Er Neutron Capture Gammas

Isotope	$E_\gamma(\text{keV})$	$\sigma_\gamma^z(b)$	$k_o$
167	79.8040(10)	18.2(8)	0.330(14)
167	184.2850(10)	56(5)	1.01(9)
167	198.2440(10)	29.9(16)	0.54(3)
167	284.6560(20)	13.7(12)	0.248(22)
167	631.7050(20)	7.9(3)	0.143(5)
167	730.6580(10)	11.6(4)	0.210(7)
167	741.3650(20)	6.72(24)	0.122(4)
167	815.9890(20)	42.5(15)	0.77(3)
167	821.1680(20)	6.2(3)	0.112(5)
167	853.4810(10)	7.5(3)	0.136(5)
167	914.9420(10)	6.99(24)	0.127(4)

429 This measured spectrum shows the prominent 1 MeV and 766 keV peaks;  
 430 particularly important for shielded configurations where the 186 keV gamma  
 431 may be significantly attenuated. The placement of a natural or even depleted  
 432 uranium source can be adjusted to match the desired photopeak ratios see in  
 433 Figure 2. Additionally, shielding could be applied to the augmenting source as  
 434 necessary, based on the characteristics of available materials.

435

#### 436 4. Conclusion

437 The research has shown for the first time that a surrogate source of rea-  
 438 sonable fidelity may be produced by exploiting the prompt gamma that results  
 439 from neutron capture. Focusing specifically on  $^{157}\text{Gd}$  as the target isotope, a  
 440 spherical configuration was used in building a prototype source. This configu-  
 441 ration features a neutron source, lead capsule, polyethylene moderator sphere,  
 442 and an gadolinium hemisphere approximately 1 mm thick. The results show  
 443 that the surrogate source has a strong peak at 181 keV that closely matches the

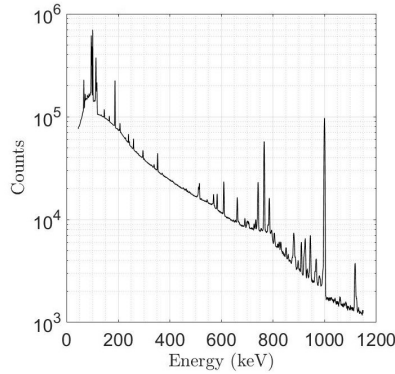


Figure 15: Depleted Uranium Spectrum

444 186 keV from  $^{235}\text{U}$ . Future tests will be performed with a more heavily shielded  
 445  $^{252}\text{Cf}$  source in order to minimize fission and decay gamma interference from  
 446 the neutron source. Further, tests will be conducted using both the prototype  
 447 configuration source and natural or depleted uranium sources combined for aug-  
 448 mentation of the high energy signature. Methods will then be repeated for the  
 449 erbium and dysprosium hemispheres, allowing for a more complete determina-  
 450 tion of the best target material for the final surrogate SNM source design. The  
 451 entire process will then be repeated in the development of a surrogate for WGPu.  
 452

### 453 Acknowledgements

454 This work was supported by funding from the United States Naval Academy's  
 455 Bowman Scholar Program.  
 456

### 457 References

- 458 [1] 2013-2014 annual report, Tech. rep., Nuclear Threat Initiative.
- 459 [2] P. Peerani, A. Tomanin, Surrogates of plutonium for detection equip-  
 460 ment testing, Nuclear Instruments and methods in Physics Research Section

- 461 A: Accelerators, Spectrometers, Detectors and Associated Equipment 654  
462 (2011) 613–620.
- 463 [3] G. W. Philips, D. J. Nagel, T. Coffey, A primer on the detection of nu-  
464 clear and radiological weapons, Tech. rep., NATIONAL DEFENSE UNIV  
465 WASHINGTON DC CENTER FOR TECHNOLOGY AND NATIONAL  
466 SECURITY POLICY (2005).
- 467 [4] M. E. Anderson, J. F. Lemming, Selected measurement data for pluto-  
468 nium and uranium, Tech. rep., Monsanto Research Corp., Miamisburg,  
469 OH (USA). Mound (1982).
- 470 [5] Evaluated nuclear structure data file search and retrieval (2017).  
471 URL <http://www.nndc.bnl.gov/ensdf/>
- 472 [6] Experimental unevaluated nuclear data list search and retrieval (2017).  
473 URL <http://www.nndc.bnl.gov/ensdf/xundl.jsp>
- 474 [7] Database of Prompt Gamma Rays from Slow Neutron Capture for Elemen-  
475 tal Analysis, International Atomic Energy Agency, Vienna, 2007.
- 476 [8] Thermal Neutron Capture Gamma Rays, International Atomic Energy  
477 Agency, 2008.  
478 URL <https://www-nds.iaea.org/capgam/index.htmlx>
- 479 [9] H. Palme, H. S. C. O'Neill, Cosmochemical estimates of mantle composi-  
480 tion, Treatise on geochemistry 2 (2003) 568.
- 481 [10] K. Rosman, P. Taylor, Isotopic compositions of the elements 1997 (technical  
482 report), Pure and Applied Chemistry 70 (1) (1998) 217–235.
- 483 [11] F. De Corte, A. Simonits, A. De Wispelaere, J. Hoste, Accuracy and appli-  
484 cability of the  $k_0$ -standardization method, Journal of Radioanalytical and  
485 Nuclear Chemistry 113 (1) (1987) 145–161.
- 486 [12] C. Werner, Mcnp users manual - code version 6.2, Tech. Rep. LA-UR-17-  
487 29981, Los Alamos National Laboratory (2017).

<sup>488</sup> [13] Prompt gamma activation analysis (2017).  
<sup>489</sup> URL <https://www-nds.iaea.org/pgaa/pgaa7/index.html>